

Finite-time dynamical phase transition in non-equilibrium relaxation

Jan Meibohm¹ and Massimiliano Esposito¹

¹*Complex Systems and Statistical Mechanics, Department of Physics and Materials Science,
University of Luxembourg, L-1511 Luxembourg, Luxembourg*

We uncover a finite-time dynamical phase transition in the thermal relaxation of a mean-field magnetic model. The phase transition manifests itself as a cusp singularity in the probability distribution of the magnetisation that forms at a critical time. The transition is due to a sudden switch in the dynamics of the system, characterised by a dynamical order parameter, and is shown to be independent of the specific details of the model. Close to criticality, we find an exact mapping between the dynamical phase transition and an equilibrium phase transition of the same model at finite external field, and thus derive dynamical critical exponents of mean-field type. We argue that spatiotemporal fluctuations of the order parameter, neglected at the mean-field level, may lead to corrections to the mean-field exponents, thus giving rise to novel, dynamical critical phenomena.

The dynamic response of many-body systems to changes of the external parameters, be it the temperature, pressure or an external field, is of fundamental interest in statistical mechanics and has a wide range of applications. When the changes are small, the response of the system is linear [1–4], and rather well understood [5–7]. In many applications, however, the external parameters switch suddenly and violently, thus driving the system far away from equilibrium. Non-equilibrium relaxation phenomena are theoretically [8–10] and experimentally [11–13] challenging, in particular when they exhibit long transients [14, 15], which is often the case in presence of phase transitions.

Equilibrium phase transitions are qualitative changes of a system’s equilibrium state under adiabatic variation of the external parameters [16]. They are accompanied by characteristic changes of order parameters [17], such as the density or the magnetisation. At continuous phase transitions, thermodynamic quantities and order parameters exhibit power-law behaviour [18], and the values of their critical exponents divide systems into universality classes. Recent developments [19–24] have given rise to conceptual generalisations of phase transitions to non-equilibrium systems [25–30] and dynamic observables [31–38]. These “dynamical phase transitions” are related to qualitative changes in the *dynamics* [39–43], observed in the long-time limit, under varying external conditions.

In this Letter, we uncover a *finite-time* dynamical phase transition in the non-equilibrium relaxation of a classical, mean-field spin model. In distinction to other classical transitions, the present one occurs in the transient response to an instantaneous change (a “quench”) of the temperature that induces an order-to-disorder phase transition. Interestingly, dynamical phase transitions with similar properties have recently been found in closed quantum systems [44, 45]. The transition manifests itself as a transient cusp singularity in the probability distribution of the magnetisation and is the result of competing dynamic behaviours within the system. The interpretation of this cusp as a phase transition sheds new light on previous works [46–51] that describe mathematical details of the singularity. We show that the transition is robust against symmetry preserving transformations, which proves its model

independence, and classify it by an exact mapping onto an equilibrium transition, yielding mean-field type critical exponents. Spatiotemporal fluctuations of the order parameter may give rise to corrections of these mean-field exponents, suggesting a new kind of dynamical critical phenomenon.

The Curie-Weiss model consists of $N \rightarrow \infty$ coupled Ising spins $\sigma_i = \pm 1$, $i = 1, \dots, N$, with infinite-range, ferromagnetic interaction of strength $J/(2N)$. The system is immersed in a heat bath at inverse temperature $\beta = 1/(k_B T)$, and subject to an external field H . Due to the mean-field nature of the interaction, all states with equal numbers N_{\pm} of spins in the states ± 1 , respectively, are equivalent. Therefore, any microstate can be written in terms of the total magnetisation $M = N_+ - N_-$. The free energy F , minimised at equilibrium, reads [17]

$$F(M) = -\frac{J}{2N} (M^2 - N) - MH - \beta^{-1} S(M), \quad (1)$$

where the first two terms are energetic contributions and the dimensionless internal entropy $S(M) = \ln \Omega(M)$ originates from the microscopic degeneracy $\Omega(M)$ of M .

We endow the system with a stochastic dynamics mediated by thermal fluctuations of the heat bath. A transition $\mp 1 \rightarrow \pm 1$ of an arbitrary spin leads to $M \rightarrow M_{\pm} \equiv M \pm 2$. The evolution of the probability $P(M, t)$ for finding the system in state M at time t is described by the master equation

$$\dot{P}(M, t) = \sum_{\pm} [W_{\pm}(M_{\mp})P(M_{\mp}, t) - W_{\pm}(M)P(M, t)], \quad (2)$$

where $W_{\pm}(M)$ are the rates for $M \rightarrow M_{\pm}$, given by

$$W_{\pm}(M) = \frac{N \mp M}{2\tau} \exp \left\{ \pm \beta \left[\frac{J}{N} (M \pm 1) + H \right] \right\}, \quad (3)$$

with microscopic relaxation time τ . The algebraic prefactor $\propto N \mp M = N_{\mp}$ is due to equivalence of microscopic transitions, and we have $W_{\pm}(M)|_{H=0} = W_{\mp}(-M)|_{H=0}$ by symmetry. Forward and backward rates are related by detailed balance [52], $W_{\pm}(M)P^{\text{eq}}(M) = W_{\mp}(M_{\pm})P^{\text{eq}}(M_{\pm})$, with respect to the equilibrium distribution $P^{\text{eq}}(M) = Z^{-1} \exp[-\beta F(M)]$; Z denotes the partition function.

To take the thermodynamic limit, $N \rightarrow \infty$, we define the intensive magnetisation $m \equiv M/N$ per spin and the free-energy density $\mathcal{F}(m) \equiv F(M)/N$. The equilibrium distribution for m then takes the large-deviation form $P^{\text{eq}}(m) \propto$

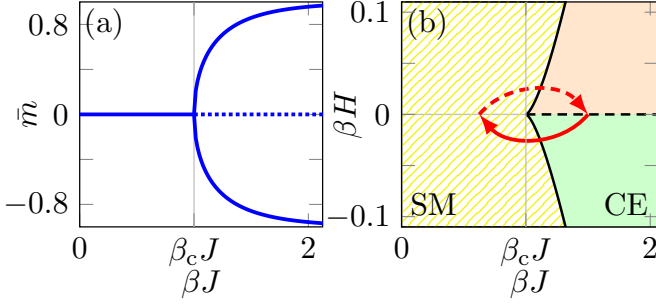


FIG. 1. (a) Magnetisation \bar{m} at $H = 0$. Solid lines correspond to minima of \mathcal{V}^{eq} , the dotted line to a local maximum. (b) Equilibrium phase diagram, featuring the SM phase (lined region) and CE phase (filled regions) separated by the phase boundary (black, solid line). At the dashed line, \bar{m} jumps discontinuously. The red arrows indicate disordering (solid) and ordering (dashed) quenches, respectively.

$\exp[-N\mathcal{V}^{\text{eq}}(m)]$ [21, 53] with equilibrium rate function $\mathcal{V}^{\text{eq}}(m) = \beta [\mathcal{F}(m) - \mathcal{F}(\bar{m})]$, where

$$\mathcal{F}(m) = -\frac{J}{2}m^2 - mH - \beta^{-1}\mathcal{S}(m), \quad (4)$$

and $\mathcal{S}(m) = -(1/2)\sum_{\pm}(1 \pm m)\ln(1 \pm m) + \ln 2$. The term $\mathcal{F}(\bar{m}) = \min_m \mathcal{F}(m)$ comes from the normalisation of $P^{\text{eq}}(M)$ and \bar{m} denotes the order parameter, the mean magnetisation $\bar{m} = \langle m \rangle$ in the large- N limit.

Expanding $\mathcal{V}^{\text{eq}}(m)$ to quartic order in m , one finds that the quadratic term changes sign at $\beta_c = 1/J$ while the quartic term remains positive. Hence, at vanishing $H = 0$, $\mathcal{V}^{\text{eq}}(m)$ passes from a single well to a symmetric double-well at the critical inverse temperature β_c . This corresponds to a continuous phase transition [54] from a disordered into an ordered state.

Close to β_c , the order parameter \bar{m} changes continuously from $\bar{m} = 0$ to finite \bar{m} , as shown in Fig. 1(a). Figure 1(b) shows the phase diagram of the model, exhibiting two distinct phases, separated by a phase boundary (solid line): a single-mode (SM) phase, where \mathcal{V}^{eq} has a unique minimum, and a coexistence (CE) phase, where local and global minima coexist. Within the CE phase, $H \neq 0$ lifts the degeneracy between the two minima in $\mathcal{V}^{\text{eq}}(m)$, and thus splits the CE phase into regions with $\bar{m} > 0$ (orange) and $\bar{m} < 0$ (green). Moving across the dashed line that separates the two, \bar{m} jumps discontinuously to $-\bar{m}$.

In the vicinity of the critical point, $(\beta, H) = (\beta_c, 0)$, we obtain from $d\mathcal{V}^{\text{eq}}(\bar{m})/dm = 0$ the equation of state

$$\beta H \sim -J(\beta - \beta_c)\bar{m} + \frac{\bar{m}^3}{3}, \quad (5)$$

which leads to the mean-field critical exponents [17, 18], universal among mean-field models: For $H = 0$, one has $\bar{m} = 0$ and $\bar{m} \propto |\beta - \beta_c|^{1/2}$, below and slightly above β_c , respectively. At $\beta = \beta_c$ and finite H , one finds the critical isotherm $H \propto \bar{m}^3$. Finally, the isothermal magnetic susceptibility $\chi_T = \partial\bar{m}/\partial H|_{H=0}$ diverges at the critical point as $\chi_T \propto |\beta - \beta_c|^{-1}$.

Starting from an ordered equilibrium state in the CE phase with $\beta > \beta_c$ at time $t < 0$, we drive the system out of equilibrium at $t = 0$ by an instantaneous disordering quench $\beta \rightarrow \beta_q$ into the SM phase, $\beta_q < \beta_c$. For simplicity, we consider vanishing external field, $H = 0$. Because the quench crosses the phase boundary [solid arrow in Fig. 1(b)], it induces an order-to-disorder phase transition. In contrast to ordering quenches [dashed arrow in Fig. 1(b)] [14], disordering quenches are ergodic, so that $P(m, t) \rightarrow P_q^{\text{eq}}(m) \propto \exp[-N\mathcal{V}_q^{\text{eq}}(m)]$ as $t \rightarrow \infty$, where $\mathcal{V}_q^{\text{eq}}(m)$ is the equilibrium rate function at the final inverse temperature β_q .

For $t > 0$, the post-quench dynamics of the probability distribution $P(m, t) \propto \exp[-NV(m, t)]$, with time-dependent rate function $V(m, t)$, is determined by Eq. (2) which turns into the Hamilton-Jacobi equation

$$0 = \partial_t V(m, t) + \mathcal{H}[m, \partial_m V(m, t)], \quad (6)$$

to leading order in $N \gg 1$, with initial condition $V(m, 0) = \mathcal{V}^{\text{eq}}(m)$ and Hamiltonian [55, 56]

$$\mathcal{H}(q, p) = w_+(q)(e^{2p} - 1) + w_-(q)(e^{-2p} - 1); \quad (7)$$

see Supplemental Information (SI) [57]. Here, $w_{\pm}(q) = (2\tau)^{-1}(1 \mp q)\exp(\pm\beta_q J q/2)$ denote the N -scaled transition rates. Solutions to Eq. (6) are given in terms of the characteristics $q(s)$ and $p(s)$, $0 \leq s \leq t$, that solve the Hamilton equations [58]

$$\dot{q}(s) = \partial_p \mathcal{H}(q, p), \quad \dot{p}(s) = -\partial_q \mathcal{H}(q, p), \quad (8)$$

with boundary conditions

$$p(0) = \frac{d}{dm} \mathcal{V}^{\text{eq}}[q(0)], \quad q(t) = m. \quad (9)$$

From the solutions of Eqs. (8)–(9), $V(m, t)$ is obtained as

$$V(m, t) = \int_0^t ds [p\dot{q} - \mathcal{H}(q, p)] + \mathcal{V}^{\text{eq}}[q(0)]. \quad (10)$$

Any solution of Eqs. (8)–(9) solves the variational problem $\delta V(m, t) = 0$, where δ denotes a variation over all trajectories with final point $q(t) = m$ [58, 59]. Hence, the characteristics $[q(s), p(s)]_{0 \leq s \leq t}$ are either minima, saddles, or maxima of Eq. (10). From the large-deviation form $P(m, t) \propto \exp[-NV(m, t)]$ we conclude that only those characteristics that minimise $V(m, t)$ can contribute for $N \rightarrow \infty$, since all other solutions are exponentially suppressed. The minimising characteristics constitute the system's optimal fluctuation, the most likely way to realise the magnetisation $q(t) = m = \lim_{N \rightarrow \infty} M(t)/N$ at time t , in response to the quench at $t = 0$.

We compute $V(m, t)$ by numerically solving Eqs. (8)–(9) using a shooting method [60] on a fine m grid, see SI. From our method we extract three fields: $V(m, t)$ [by evaluating Eq. (10)], the derivative field $\partial_m V(m, t) = p(t)$ [the end point of $p(s)$], and the initial magnetisation $m_0(m, t) = q(0)$ [the initial point of $q(s)$].

The blue curves in Fig. 2(a) show $V(m, t)$ for different t ; the green and red curves show \mathcal{V}^{eq} and $\mathcal{V}_q^{\text{eq}}$, respectively. For

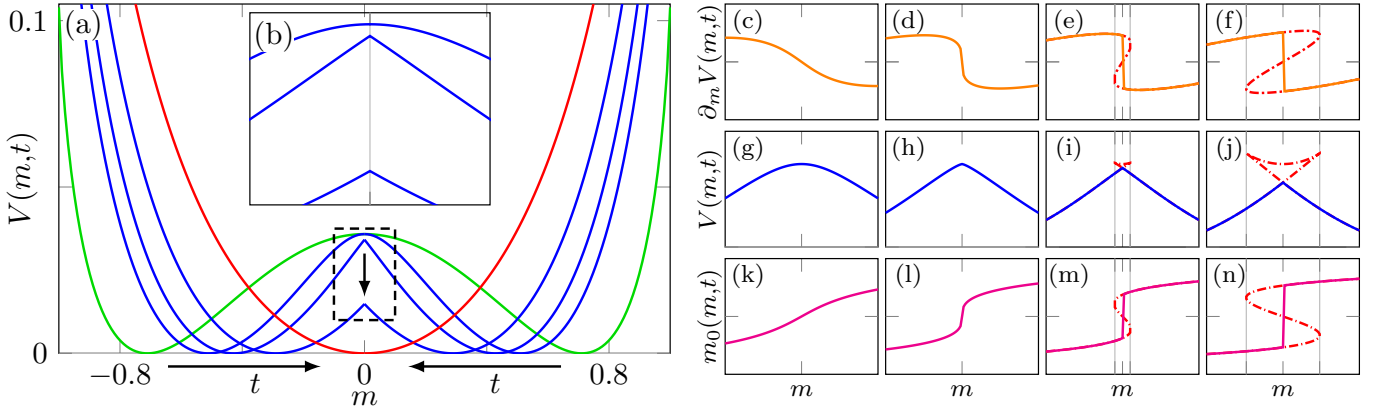


FIG. 2. Post-quench dynamics for $\beta = 1.25/J$ and $\beta_q = 0.75/J$. (a) Rate functions \mathcal{V}^{eq} (green), $\mathcal{V}_q^{\text{eq}}$ (red), and $V(m,t)$ for $t/\tau = 0.25, 0.4$ and 1.25 (blue). The black arrows indicate the change of $V(m,t)$ in time. (b) Magnification of the dashed rectangle in Fig. 2(a). (c)–(n) Time-evolution of $\partial_m V(m,t)$ [(c)–(f)], $V(m,t)$ [(g)–(j)] and $m_0(m,t)$ [(k)–(n)] for $t/\tau = 0.25, 0.35, 0.4$, and 0.5 (from left to right). The solid and dash-dotted lines show the leading and sub-leading solutions, respectively (see main text). The gray lines delimit the coexistence region.

small times, $V(m,t)$ has the shape of a symmetric double well, inherited from the initial \mathcal{V}^{eq} . As t increases, the minima of $V(m,t)$ move towards the origin, and the local maximum at $m=0$ decreases, as indicated by the black arrows in Fig. 2(a). In the long-time limit, $V(m,t)$ approaches the single-mode shape of $\mathcal{V}_q^{\text{eq}}$.

Notably, however, $V(m,t)$ does not evolve smoothly: At a finite time t , $V(m,t)$ forms a cusp at $m=0$ [see Fig. 2(b)], and the derivative field $\partial_m V(m,t)$ develops a discontinuous jump. The origin of this jump is shown in Figs. 2(c)–(f): As time evolves, $\partial_m V(m,t)$ folds over and becomes multi-valued, and up to three solutions of Eqs. (8)–(9) coexist within a finite interval, delimited by the gray lines in Figs. 2(e) and (f). Out of these solutions, we select the one with smallest $V(m,t)$, which naturally leads to a Maxwell construction for the leading solution, shown in orange. The sub-leading solutions [red, dash-dotted curves in Fig. 2(c)–(f)] have a larger $V(m,t)$ as shown in Figs. 2(g)–(j). Figures 2(k)–(n) indicate the same multivaluedness and an analogous Maxwell construction for $m_0(m,t)$, culminating in a discontinuous jump at $m=0$.

Interpreting the formation of the cusp as a finite-time dynamical phase transition, we exploit the similarities with the equilibrium transition of the model. We first note that the sudden change of m_0 at $m=0$ is strikingly similar to the discontinuous jump of \bar{m} at equilibrium, when the external field H crosses zero in the CE phase [dashed line in Fig. 1(b)]. To be specific, we identify t , m_0 and m in the dynamical case with β , \bar{m} and H , respectively, at equilibrium, and draw a “dynamical phase diagram”, shown in Figure 3(a): Small times $t < t_c$ correspond to the dynamical single-mode (DSM) phase (yellow, lined region) where the dynamical order parameter $m_0(m,t)$ is unique (just like \bar{m} for $\beta < \beta_c$) and $V(m,t)$ is a smooth function of m . For $t > t_c$ the system transitions into a dynamical coexistence (DCE) phase (filled region) where multiple m_0 values coexist. The DCE phase corresponds to the m interval delimited by the gray lines in Figs. 2(m) and (n). For $m=0$, the two values, m_0 and $-m_0$ are degenerate, in analogy with \bar{m} and $-\bar{m}$

for $\beta > \beta_c$ and $H=0$. Conditioning on $m \neq 0$ lifts this degeneracy, so that one of the m_0 values becomes exponentially suppressed. As a consequence, when crossing the dashed line in the DCE phase in Fig. 3(a), m_0 jumps discontinuously, leading to the kink in $V(m,t)$ at $m=0$.

On the trajectory level, the transition from the DSM into the DCE phase corresponds to a sudden change of the optimal fluctuation that minimises $V(m,t)$ in Eq. (10) [48, 49]. This follows from the dynamical analogue of an energy-entropy argument [18]: For small times, the right-hand side of Eq. (10) is dominated by the first term, interpreted as a dynamical activity, that is minimised by the inactive solution $p(s) = q(s) = 0$, but at the cost of an unfavourable initial $m_0 = q(0) = 0$, the local maximum of \mathcal{V}^{eq} . For long times, the activity-term loses its dominance and the static second term becomes important. Consequently, the optimal fluctuation optimises m_0 , and starts at the minima of \mathcal{V}^{eq} .

To visualise the role of the optimal fluctuation, we perform numerical simulations at finite N . Using Eq. (2), we generate a large number of trajectories and record $q(s) \approx M(s)/N$, for different $0 \leq s \leq t$, conditioning the trajectories to end up at $q(t) \in [m - dm, m + dm]$ for given t and m , and a small dm . We then collect histograms of $q(s)$, normalised to unity for each s , and merge them, to obtain a numerical approximation of the trajectory density, shown in Figs. 3(b)–(e). The colour coding matches the corresponding values for t and m , shown as the equally-coloured dots in Fig. 3(a).

Figures 3(b) and (c) show good agreement between the optimal fluctuations (solid, black lines) and the yellow regions of high trajectory density in the DSM and DCE phase, respectively, at $m=0$. In the DSM phase [Fig. 3(b)], we observe a unique optimal fluctuation that remains at zero, the inactive solution. Beyond the dynamical critical point [Fig. 3(c)], two degenerate optimal fluctuations coexist, with initial magnetisations m_0 and $-m_0$ close to the minima of \mathcal{V}^{eq} . The third trajectory (dotted line) is a local maximum of $V(m,t)$, and not observed in the numerics.

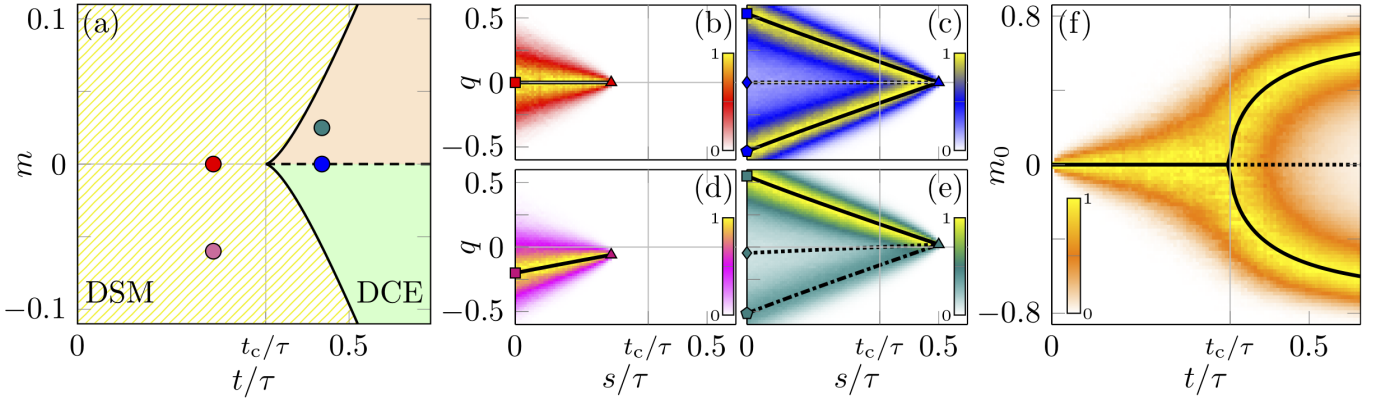


FIG. 3. (a) Dynamical phase diagram for $(\beta, \beta_q) = (1.25/J, 0.75/J)$, featuring the DSM (yellow, lined region) and DCE (filled region) phases (see main text), separated by a phase boundary (solid line). The DCE phase splits into regions with $m_0 > 0$ (orange) and $m_0 < 0$ (green), separated by the dashed line, where m_0 jumps discontinuously. The coloured circles correspond to the parameter values of the equally coloured trajectory densities in Fig. 3(b)–(e). (b)–(e) Optimal fluctuations from Eqs. (8)–(9) (solid, black lines) and from numerical simulation of Eq. (2) (coloured regions, obtained with $N = 200$ using 10^8 trajectories). Colour coding according to the (t, m) values of the equally coloured bullets in Fig. 3(a). Sub-leading trajectories are shown as broken lines, symbols mark $m_0 = q(0)$ and $m = q(t)$. (f) Density of m_0 at $m = 0$ as function of t from numerical simulations (coloured region, obtained with $N = 200$ using 10^8 trajectories) and from theory (solid lines). The dotted line shows the sub-leading m_0 .

Figures 3(d) and (e) show the optimal fluctuations and trajectory densities for finite m . In the DSM phase [Fig. 3(d)], the conditioning shifts the optimal fluctuation away from zero. Finite m in the DCE phase [Fig. 3(e)] lifts the degeneracy between the optimal fluctuations, so that one of them is degraded to a local minimum of $V(m, t)$ (dash-dotted line), whose remnants are still visible in the trajectory density at finite N .

In Fig. 1(f) we visualise the dependence of the order parameter m_0 on t by joining the histograms of $m_0 = q(0) \approx M(0)/N$ for different t . The black, solid line shows the theoretical prediction for m_0 , obtained from Eqs. (8)–(9). Apart from the excellent agreement between the yellow regions and the theoretical curves, we observe a close similarity with the dependence of \bar{m} on β , see Fig. 1(a).

To classify the dynamical phase transition in terms of equilibrium categories, we now show that close to the critical point, the dynamical phase diagram can be exactly mapped onto the equilibrium one, so that the dynamical critical exponents of both match. We first calculate the critical time t_c at which m_0 becomes multi-valued for $m = 0$. Since $V(0, t)$ develops a kink at time $t = t_c$, the curvature $z(t) = \partial_m^2 V(0, t)$ must tend to negative infinity, $z(t) \rightarrow -\infty$ as $t \rightarrow t_c$. Taking a partial derivative of Eq. (8), we find that $z(t)$ obeys the Riccati equation $\tau \dot{z}(t) = -4J(\beta_c - \beta_q)z(t) - 4z(t)^2$ with initial condition $z(0) = -J(\beta - \beta_c)/2$ (see SI). The solution $z(t)$ tends to $-\infty$ at the finite time $t_c/\tau = \ln[(\beta - \beta_q)/(\beta - \beta_c)]/[4(\beta_c - \beta_q)J]$, obtained with a different method in Ref. [48]. For the parameters used in Figs. 2 and 3, we have $t_c/\tau = \ln(2) \approx 0.3465$, in agreement with the numerical result. Symmetry-preserving transformations of the rates $W_{\pm}(M) \rightarrow \tilde{W}_{\pm}(M)$ lead to $\mathcal{H}(q, p) \rightarrow f(q)\mathcal{H}(q, p)$, for an even function f with $f(0) = 1$ (see SI). Consequently, any such transformation leaves t_c invariant, i.e., the transition does not depend on the model-specific form of

$W_{\pm}(M)$.

From Eq. (8)–(9) we now derive the dynamical analogue of the equation of state (5). We first note that close to the critical point $m_0 \ll 1$ and $m \ll 1$, so that $q(s), p(s) \ll 1$ along the trajectory. This allows us to expand the Hamiltonian \mathcal{H} to fourth order in q and p . We obtain $\mathcal{H} \sim \mathcal{H}_0 + \mathcal{H}_1$, with the quadratic and quartic Hamiltonians \mathcal{H}_0 and \mathcal{H}_1 , respectively. Since $\mathcal{H}_0 \gg \mathcal{H}_1$, we solve Eq. (8)–(9) perturbatively, leading to the dynamical equation of state

$$m \sim -[a_1 \tau^{-1}(t - t_c) + \dots]m_0 + (b_0 + \dots)m_0^3, \quad (11)$$

where $a_1 > 0$ and $b_0 > 0$ for $\beta < 3/(2J)$, and arbitrary β_q and J ; the dots denote higher-order terms in $t - t_c$ (see SI). Comparing with Eq. (5), we conclude that both equations can be mapped onto each other by proper rescaling of, e.g., $t - t_c$, m_0 and m , so that the dynamical phase transition has mean-field critical exponents. This shows that the transition is continuous, since m_0 changes continuously from $m_0 = 0$ for $t < t_c$ to $m_0 \propto |t - t_c|^{1/2}$ above t_c . By contrast, for $\beta > 3/(2J)$ the system undergoes a discontinuous, first-order dynamical phase transition, where m_0 jumps discontinuously. In this case, the fields $V(m, t)$, $\partial_m V(m, t)$ and $m_0(m, t)$ acquire a more complicated “fine structure” of folds which forms at times $t < t_c$.

Close to the critical point, spatiotemporal fluctuations of m_0 , neglected in our model, may give rise to corrections to the mean-field exponents [17, 18]. Since the fluctuations are of dynamical origin, we hypothesise that these corrections will be different from the equilibrium ones, and thus reflect a novel, dynamical critical phenomenon. This can be tested by investigating the post-quench dynamics of systems with short-range interactions in two and three dimensions using Monte-Carlo simulations [61], or perhaps dynamic renormalisation group methods [62].

We thank Gianmaria Falasco and Nahuel Freitas for discussions, and Karel Proesmans for pointing out the connection with the mathematics literature. This work was supported by the European Research Council, project NanoThermo (ERC-2015-CoG Agreement No. 681456).

-
- [1] L. Onsager, Phys. Rev. **37**, 405 (1931).
 [2] L. Onsager, Phys. Rev. **38**, 2265 (1931).
 [3] R. Kubo, J. Phys. Soc. Japan **12**, 570 (1957).
 [4] R. Kubo, M. Yokota, and S. Nakajima, J. Phys. Soc. Japan **12**, 1203 (1957).
 [5] R. Chetrite, Phys. Rev. E **80**, 051107 (2009).
 [6] G. Falasco and M. Baiesi, New J. Phys. **18**, 43039 (2016).
 [7] M. Baiesi and C. Maes, New J. Phys. **15**, 13004 (2013).
 [8] I. M. Lifshitz, Sov. Phys. JETP **15**, 939 (1962).
 [9] R. G. Palmer, D. L. Stein, E. Abrahams, and P. W. Anderson, Phys. Rev. Lett. **53**, 958 (1984).
 [10] L. F. Cugliandolo, in *Slow Relaxations nonequilibrium Dyn. Condens. matter* (Springer, 2003) pp. 367–521.
 [11] E. R. Weeks and D. A. Weitz, Phys. Rev. Lett. **89**, 095704 (2002).
 [12] P. Wang, C. Song, and H. A. Makse, Nat. Phys. **2**, 526 (2006).
 [13] A. Farhan, P. M. Derlet, A. Kleibert, A. Balan, R. V. Chopdekar, M. Wyss, J. Perron, A. Scholl, F. Nolting, and L. J. Heyderman, Phys. Rev. Lett. **111**, 057204 (2013).
 [14] A. J. Bray, Adv. Phys. **51**, 481 (2002).
 [15] L. Berthier and G. Biroli, Rev. Mod. Phys. **83**, 587 (2011).
 [16] H. B. Callen, *Thermodynamics and an Introduction to Thermostatistics, 2nd Edition*, 2nd ed. (John Wiley & Sons, New York, 1985).
 [17] P. M. Chaikin, T. C. Lubensky, and T. A. Witten, *Principles of condensed matter physics*, Vol. 10 (Cambridge University Press, Cambridge, 1995).
 [18] N. Goldenfeld, *Lectures on phase transitions and the renormalization group* (CRC Press, Boca Raton, 1992).
 [19] M. I. Freidlin and A. D. Wentzell, *Random perturbations of dynamical systems* (Springer, New York, USA, 1984).
 [20] R. Graham and T. Tél, Phys. Rev. Lett. **52**, 9 (1984).
 [21] R. S. Ellis, *Entropy, large deviations, and statistical mechanics* (Springer, 2007).
 [22] U. Seifert, Reports Prog. Phys. **75**, 126001 (2012).
 [23] L. Bertini, A. De Sole, D. Gabrielli, G. Jona-Lasinio, and C. Landim, Rev. Mod. Phys. **87**, 593 (2015).
 [24] L. Peliti and S. Pigolotti, *Stochastic Thermodynamics: An Introduction* (Princeton University Press, 2021).
 [25] B. Derrida, J. Phys. A: Math. Gen. **20**, L721 (1987).
 [26] H. Ge and H. Qian, J. R. Soc. Interface **8**, 107 (2011).
 [27] T. Tomé and M. J. de Oliveira, Phys. Rev. Lett. **108**, 020601 (2012).
 [28] T. Herpich, J. Thingna, and M. Esposito, Phys. Rev. X **8**, 031056 (2018).
 [29] H. Vroylandt, M. Esposito, and G. Verley, Phys. Rev. Lett. **124**, 250603 (2020).
 [30] T. Martynec, S. H. L. Klapp, and S. A. M. Loos, New J. Phys. **22**, 93069 (2020).
 [31] J. Mehl, T. Speck, and U. Seifert, Phys. Rev. E **78**, 011123 (2008).
 [32] D. Lacoste, A. W. C. Lau, and K. Mallick, Phys. Rev. E **78**, 011915 (2008).
 [33] R. L. Jack and P. Sollich, Prog. Theor. Phys. Suppl. **184**, 304 (2010).
 [34] P. T. Nyawo and H. Touchette, EPL (Europhysics Lett. **116**, 50009 (2017).
 [35] T. Nemoto, É. Fodor, M. E. Cates, R. L. Jack, and J. Tailleur, Phys. Rev. E **99**, 022605 (2019).
 [36] A. Lazarescu, T. Cossetto, G. Falasco, and M. Esposito, J. Chem. Phys. **151**, 64117 (2019).
 [37] M. Suñé and A. Imparato, Phys. Rev. Lett. **123**, 070601 (2019).
 [38] T. Herpich, T. Cossetto, G. Falasco, and M. Esposito, New J. Phys. **22**, 63005 (2020).
 [39] J. P. Garrahan, R. L. Jack, V. Lecomte, E. Pitard, K. van Duivendijk, and F. van Wijland, Phys. Rev. Lett. **98**, 195702 (2007).
 [40] P. T. Nyawo and H. Touchette, Phys. Rev. E **98**, 052103 (2018).
 [41] R. L. Jack, Eur. Phys. J. B **93**, 1 (2020).
 [42] K. Proesmans, R. Toral, and C. den Broeck, Phys. A Stat. Mech. its Appl. **552**, 121934 (2020).
 [43] Y.-E. Keta, É. Fodor, F. van Wijland, M. E. Cates, and R. L. Jack, Phys. Rev. E **103**, 022603 (2021).
 [44] M. Heyl, A. Polkovnikov, and S. Kehrein, Phys. Rev. Lett. **110**, 135704 (2013).
 [45] M. Heyl, Reports Prog. Phys. **81**, 54001 (2018).
 [46] A. van Enter, R. Fernández, F. den Hollander, and F. Redig, Commun. Math. Phys. **226**, 101 (2002).
 [47] C. Külske and A. Le Ny, Commun. Math. Phys. **271**, 431 (2007).
 [48] A. C. D. van Enter, R. Fernández, F. Den Hollander, and F. Redig, Moscow Math. J. **10**, 687 (2010).
 [49] V. Ermolaev and C. Külske, J. Stat. Phys. **141**, 727 (2010).
 [50] F. Redig and F. Wang, J. Stat. Phys. **147**, 1094 (2012).
 [51] R. Fernández, F. den Hollander, and J. Martínez, Commun. Math. Phys. **319**, 703 (2013).
 [52] N. Van Kampen, in *Stoch. Process. Phys. Chem.* (Elsevier, 2007).
 [53] H. Touchette, Phys. Rep. **478**, 1 (2009).
 [54] L. D. Landau, Zh. Eksp. Teor. Fiz. **11**, 19 (1937).
 [55] M. I. Dykman, E. Mori, J. Ross, and P. M. Hunt, J. Chem. Phys. **100**, 5735 (1994).
 [56] J. Feng and T. G. Kurtz, *Large deviations for stochastic processes*, 131 (American Mathematical Soc., 2006).
 [57] See Supplemental Information at [...] for additional details on mathematical derivations and our numerical method, as well as on the generality and robustness of our results, which includes Refs. [63–67].
 [58] R. Courant and D. Hilbert, *Methods of mathematical physics, Volume II* (John Wiley & Sons, 1962).
 [59] H. Goldstein, *Classical Mechanics*, 2nd ed. (Addison-Wesley, Reading, USA, 1980).
 [60] W. H. Press, W. T. Vetterling, S. A. Teukolsky, and B. P. Flannery, *Numerical recipes*, Vol. 818 (Cambridge University Press, Cambridge, 1986).
 [61] D. Landau and K. Binder, *A guide to Monte Carlo simulations in statistical physics* (Cambridge university press, 2014).
 [62] U. C. Täuber, *Critical Dynamics: A Field Theory Approach to Equilibrium and Non-Equilibrium Scaling Behavior* (Cambridge University Press, Cambridge, 2014).
 [63] V. A. Kulkarny and B. S. White, Phys. Fluids **25**, 1770 (1982).
 [64] M. Wilkinson and B. Mehlig, Europhys. Lett. **71**, 186 (2005).
 [65] J. Meibohm, K. Gustavsson, J. Bec, and B. Mehlig, New J. Phys. **22**, 13033 (2020).
 [66] M. V. Berry and C. Upstill, Prog. Opt. **18**, 257 (1980).
 [67] C. M. Bender and S. A. Orszag, *Advanced Mathematical Methods for Scientists and Engineers* (McGraw-Hill, New York, USA, 1978).

Supplemental Information for: Finite-time dynamical phase transition in non-equilibrium relaxation

Jan Meibohm¹ and Massimiliano Esposito¹

¹*Complex Systems and Statistical Mechanics, Department of Physics and Materials Science,
University of Luxembourg, L-1511 Luxembourg, Luxembourg*

In this Supplemental Information, we give additional details on the derivations and the numerical method discussed in the main text. We first derive the Hamilton-Jacobi equation [Eq. (6) in the main text] and explain the shooting method we use to solve it. From the Hamilton equations we then derive the Riccati equation for the curvature $z(t)$. Using this result, we show that the dynamical phase transition is robust against transformations of the transition rates. Finally, we show how to obtain the dynamical equation of state [Eq. (11) in the main text] by perturbing the linearised Hamilton equations.

I. DERIVATION OF HAMILTON-JACOBI EQUATION FOR $V(m, t)$

In this section, we derive the Hamilton-Jacobi equation for $V(m, t)$, Eq. (6) in the main text, from the master equation, Eq. (2) in the main text, for $P(M, t)$. The latter equation reads

$$\dot{P}(M, t) = \sum_{\pm} [W_{\pm}(M_{\mp})P(M_{\mp}, t) - W_{\pm}(M)P(M, t)], \quad \text{with rates} \quad W_{\pm}(M) = \frac{N \mp M}{2\tau} \exp \left\{ \pm \beta_q \left[\frac{J}{N} (M \pm 1) + H \right] \right\}, \quad (\text{S1})$$

where $M_{\pm} = M \pm 2$. We substitute the large-deviation Ansatz $P(M, t) \propto \exp[-NV(m, t)]$ with $m = M/N$ into Eq. (S1) and obtain

$$-\partial_t V(m, t) = \frac{1}{N} \sum_{\pm} \left\{ W_{\pm} \left[N \left(m \mp \frac{2}{N} \right) \right] \exp \left[NV(m, t) - NV \left(m \mp \frac{2}{N}, t \right) \right] - W_{\pm}(Nm) \right\}. \quad (\text{S2})$$

For $N \rightarrow \infty$, we find the limits

$$N \left[V(m, t) - V \left(m \mp \frac{2}{N}, t \right) \right] \rightarrow \pm 2 \partial_m V(m, t), \quad (\text{S3})$$

and

$$\frac{W_{\pm}(Nm)}{N} = \frac{1 \mp m}{2\tau} \exp \left\{ \pm \beta_q \left[J \left(m \pm \frac{1}{N} \right) + H \right] \right\} \rightarrow \frac{1 \mp m}{2\tau} \exp [\pm \beta_q (Jm + H)] \equiv w_{\pm}(m). \quad (\text{S4})$$

Using these limits we obtain from Eq. (S2) in the limit $N \rightarrow \infty$,

$$-\partial_t V(m, t) = \sum_{\pm} w_{\pm}(m) \{ \exp [\pm 2 \partial_m V(m, t)] - 1 \}. \quad (\text{S5})$$

Equation (S5) is a first-order partial differential equation for $V(m, t)$ which does not depend explicitly on $V(m, t)$ itself, but only on its partial derivatives. This characterises Eq. (S5) as a Hamilton-Jacobi equation [1] with Hamiltonian $\mathcal{H}(q, p)$ given in Eq. (7) in the main text. The characteristics of Eq. (S5) solve the Hamilton equations, Eq. (8) in the main text. From the conjugate momentum $p(s) = \partial_m V[q(s), s]$ one obtains the boundary condition $p(0) = \partial_m V[q(0), 0] = d\mathcal{V}^{\text{eq}}[q(0)]/dm$. Furthermore, we have

$$\frac{d}{ds} V[q(s), s] = p(s) \dot{q}(s) + \partial_s V[q(s), s] = p(s) \dot{q}(s) - \mathcal{H}[q(s), p(s)], \quad (\text{S6})$$

where we used the Hamilton-Jacobi equation in the second step. Integrating s from 0 to t we readily obtain Eq. (10) in the main text.

II. NUMERICAL SOLUTION OF HAMILTON-JACOBI EQUATION

In this section, we provide details on the numerical method used to calculate $V(m, t)$, $\partial_m V(m, t)$ and $m_0(m, t)$, shown in Fig. 2 of the main text. The Hamilton equations with boundary conditions,

$$\dot{q}(s) = \partial_p \mathcal{H}(q, p), \quad \dot{p}(s) = -\partial_q \mathcal{H}(q, p), \quad p(0) = \frac{d}{dm} \mathcal{V}^{\text{eq}}[q(0)], \quad q(t) = m, \quad (\text{S7})$$

Eqs. (8) and (9) in the main text, are fixed by two boundary conditions, at $s = 0$ and $s = t$. This classifies Eqs. (S7) as a two-point boundary value problem [2] on the finite interval $q \in [-1, 1]$. Problems of this kind can be solved to high accuracy by shooting [2].

The basic idea is the following: We numerically integrate the Hamilton equations in Eqs. (S7) for a grid of initial values

$$q^{(i)}(0) = m_0^{(i)} \in [-1, 1], \quad \text{and} \quad p^{(i)}(0) = \frac{d}{dm} \mathcal{V}^{\text{eq}}[m_0^{(i)}], \quad i = 1, \dots, M, \quad (\text{S8})$$

over given finite time t . For each grid index i , we obtain a trajectory $[q^{(i)}(s), p^{(i)}(s)]_{0 \leq s \leq t}$ with end point $[q^{(i)}(t), p^{(i)}(t)]$. For a given m , the value $\varepsilon^{(i)} = |q^{(i)}(t) - m|$ defines the error of the initial condition $m_0^{(i)}$. We use an interpolation algorithm to compute the function $\varepsilon(m_0)$, of which we numerically determine the roots m_0^* , $\varepsilon(m_0^*) = 0$. Now, we use $q(0) = m_0^*$, $p(0) = d\mathcal{V}^{\text{eq}}[m_0^*]/dm$ as initial conditions to generate the characteristic $[q(s), p(s)]_{0 \leq s \leq t}$ with error $\varepsilon = |q(t) - m|$.

Iterating this procedure for an ever finer grid on an ever smaller interval around the exact value of m_0 , we can achieve an error smaller than a given threshold, ε_{\min} . We use the standard ODE solver “ode45” in MatLab with non-default accuracy settings ‘RelTol’= 10^{-12} and ‘AbsTol’= 10^{-16} to integrate Eqs. (S7). We take $M = 10^2$ and devise an iterative procedure that reduces the interval size around m_0 by a factor of five in each iteration, until an error smaller than $\varepsilon_{\min} = 10^{-10}$ is achieved.

This program is repeated for a grid of m and t values for each of which $V(m, t)$ is computed from Eq. (10) in the main text. The two other fields, $\partial_m V(m, t)$ and $m_0(m, t)$, are evaluated directly from the end and starting points of the characteristics, $p(t)$ and $q(0)$, respectively.

III. DERIVATION AND SOLUTION OF RICCATI EQUATION FOR $z(t)$

Here we derive an equation for the curvature $z(t) = \partial_m^2 V(0, t)$ at $m = 0$, which tends to negative infinite at time t_c when $V(m, t)$ develops a kink at $m = 0$. To obtain this equation, we use $p(s) = \partial_m V[q(s), s]$ to write the Hamilton equation $\dot{p} = -\partial_q \mathcal{H}(q, p)$ as

$$\partial_m^2 V(m, t) \partial_p \mathcal{H}[m, \partial_m V(m, t)] + \partial_m \partial_t V(m, t) = -\partial_q \mathcal{H}[m, \partial_m V(m, t)], \quad (\text{S9})$$

where we evaluated the equation at t with $q(t) = m$. We take a partial derivative with respect to m to obtain

$$\begin{aligned} \partial_m^3 V(m, t) \partial_p \mathcal{H}[m, \partial_m V(m, t)] + \partial_m^2 V(m, t) \{ \partial_q \partial_p \mathcal{H}[m, \partial_m V(m, t)] + \partial_p^2 \mathcal{H}[m, \partial_m V(m, t)] \partial_m^2 V(m, t) \} + \partial_m^2 \partial_t V(m, t) = \\ - \partial_q^2 \mathcal{H}[m, \partial_m V(m, t)] - \partial_p \partial_q \mathcal{H}[m, \partial_m V(m, t)] \partial_m^2 V(m, t), \end{aligned} \quad (\text{S10})$$

We swap the order of the partial derivatives and evaluate (S10) along a trajectory $m = q(s)$ at $t = s$ to obtain an equation for $Z(s) = \partial_m^2 V[q(s), s]$. We use

$$\dot{Z}(s) = \frac{d}{ds} \partial_m^2 V[q(s), s] = \partial_m^3 V[q(s), t] \dot{q}(s) + \partial_s \partial_m^2 V[q(s), s], \quad (\text{S11})$$

to write Eq. (S10) as the Riccati equation

$$\dot{Z}(s) = -\partial_q^2 \mathcal{H}[q(s), p(s)] - 2\partial_q \partial_p \mathcal{H}[q(s), p(s)] Z(s) - \partial_p^2 \mathcal{H}[q(s), p(s)] Z(s)^2, \quad (\text{S12})$$

with initial condition $Z(0) = \partial_m^2 V[q(0), 0] = \frac{d^2}{dm^2} \mathcal{V}^{\text{eq}}[q(0)]$. Along the trajectory $q(s) = p(s) = 0$ and evaluating at $s = t$ this simplifies to an equation for $z(t) = \partial_m^2 V(0, t)$,

$$\dot{z}(t) = -\partial_q^2 \mathcal{H}(0, 0) - 2\partial_q \partial_p \mathcal{H}(0, 0) z(t) - \partial_p^2 \mathcal{H}(0, 0) z(t)^2. \quad (\text{S13})$$

Using $\partial_q^2 \mathcal{H}(0, 0) = 0$, $\partial_q \partial_p \mathcal{H}(0, 0) = 2(\beta_q J - 1)/\tau = -2J(\beta_c - \beta_q)/\tau =$ and $\partial_p^2 \mathcal{H}(0, 0) = 4/\tau$, we obtain the Riccati equation stated in the main text with initial condition

$$z(0) = \partial_m^2 V(0, 0) = \frac{d^2}{dm^2} \mathcal{V}^{\text{eq}}(0) = -J(\beta - \beta_c), \quad (\text{S14})$$

as stated in the main text. The solution $z(t)$ to Eq. (S13) then reads

$$z(t) = \frac{J(\beta - \beta_c)(\beta_c - \beta_q)}{\beta - \beta_c - (\beta - \beta_q)e^{-4J(\beta_c - \beta_q)t}}. \quad (\text{S15})$$

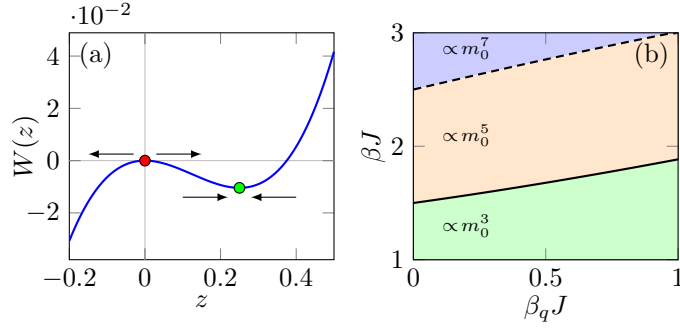


FIG. 1. (a) Potential $W(z)$ for $\beta = 1.25/J$ and $\beta_q = 0.75/J$. The arrows indicate the (in)stability of the fixed points (coloured bullets). (b) Diagram showing the values for β_q and β where terms of order m_0^3 , m_0^5 and m_0^7 must be included in the dynamical equation of state, Eq. (S32).

When $\beta > \beta_c$ and $\beta_q < \beta_c$, i.e., a disordering quench, the denominator in Eq. (S15) tends to zero, and $z(t)$ tends to $-\infty$, at the finite time

$$t_c = \frac{\tau}{4J(\beta_c - \beta_q)} \ln \left[\frac{\beta - \beta_q}{\beta - \beta_c} \right], \quad (\text{S16})$$

as stated in the main text. Unstable gradients described by Riccati equations are common in problems where so-called “caustics” form [3–5]. Conventional caustics are singularities caused by the partial focusing of light in ray optics [6]. In the present problem, analogous caustics occur as partial focuses of the characteristics $[q(s), p(s)]_{0 \leq s \leq t}$ for varying $q(0) = m_0$, whenever characteristics cross in space, indicated by $Z(s) \rightarrow -\infty$. Because points of crossing characteristics correspond to the phase boundaries in our problem, we use Eq. (S12) together with the Hamilton equations to obtain numerically accurate dynamical phase diagrams, Figs. 3(a) and (f) in the main text.

The instability of the Riccati equation (S13) for $z(t)$ can be visualised by writing $\dot{z}(t) = -W'[z(t)]$ with potential $W(z) = 4/(3\tau)z^3 - 2J(\beta_c - \beta_q)/\tau z^2$. Figure 1(a) shows $W(z)$, with stable and unstable fixed points shown as the red and green dots, respectively. Since $W(z)$ is decreasing for $z \leq 0$, any negative initial $z(0)$ leads to $z(t) \rightarrow -\infty$, at the finite time t_c , and $V(m, t)$ forms a kink at zero. For any positive initial $z(0)$, on the other hand, $z(t)$ tends to the stable fixed point (green bullet), corresponding to the curvature of $\mathcal{V}_q^{\text{eq}}(m)$ at $m = 0$. For a disordering quench with $\beta_q < \beta_c < \beta$, $z(0)$ is always negative, so that the kink of $V(m, t)$ at $m = 0$ always forms.

IV. DYNAMICAL PHASE TRANSITION UNDER CHANGE OF RATES

In this section, we use the results of Sec. III to show that the dynamical phase transition is robust against transformations of the microscopic transition rates $W_{\pm}(M)$, given in Eq. (S1) [Eq. (3) in the main text], that preserve detailed balance and the symmetry of the problem:

$$W_{\pm}(M)P^{\text{eq}}(M) = W_{\mp}(M_{\pm})P^{\text{eq}}(M_{\pm}) \quad \text{and} \quad W_{\pm}(M)|_{H=0} = W_{\mp}(-M)|_{H=0}. \quad (\text{S17})$$

These requirements do not determine $W_{\pm}(M)$ uniquely. For any (local) transformation of the rates

$$W_{\pm}(M) \rightarrow \tilde{W}_{\pm}(M) = W_{\pm}(M)F_{\pm}(M), \quad (\text{S18})$$

the same conditions (S17) are satisfied by $\tilde{W}_{\pm}(M)$ as long as

$$F_{\pm}(M) = F_{\mp}(M_{\pm}) = F_{\mp}(M \pm 2) \quad \text{and} \quad F_{\pm}(M) = F_{\mp}(-M). \quad (\text{S19})$$

We now show that the occurrence of the dynamical phase transition is robust against any such transformation.

To this end, we define $f_{\pm}(m) \equiv F_{\pm}(Nm)$ and note that as $N \rightarrow \infty$ one has $f_{\pm}(m) = F_{\pm}(Nm) = F_{\mp}[N(m \pm 2/N)] \sim F_{\mp}(Nm) = f_{\mp}(m)$, so that $f_{\pm}(m) = f_{\mp}(m) \equiv f(m)$. In other words, for $N \rightarrow \infty$, f must be independent of the direction \pm of the transition.

Second, the symmetry condition $F_{\pm}(M) = F_{\mp}(-M)$ shows that f is even, $f(m) = f(-m)$. Third, a constant $f(m) = c$ leads to a mere rescaling of the microscopic transition time τ , so that we may set $f(0) = 1$ without loss of generality.

Hence, in terms of the N -scaled rates $w_{\pm}(q)$, an arbitrary, symmetry preserving transformation reads $w_{\pm}(q) \rightarrow \tilde{w}_{\pm}(q) = f(q)w_{\pm}(q)$. Therefore, the corresponding Hamiltonian $\mathcal{H}(q, p)$ transforms as

$$\mathcal{H}(q, p) \rightarrow \tilde{\mathcal{H}}(q, p) = f(q)\mathcal{H}(q, p), \quad (\text{S20})$$

as stated in the main text. Regarding the Riccati equation (S13), we now observe that

$$\partial_q^2 \tilde{\mathcal{H}}(0,0) = \partial_q^2 \mathcal{H}(0,0) = 0, \quad \partial_q \partial_p \tilde{\mathcal{H}}(0,0) = \partial_q \partial_p \mathcal{H}(0,0) = -2J(\beta_c - \beta_q)/\tau, \quad \partial_p^2 \tilde{\mathcal{H}}(0,0) = \partial_p^2 \mathcal{H}(0,0) = 4/\tau, \quad (\text{S21})$$

where we used $f(0) = 1$ and $f'(0) = 0$, due to the above considerations. Hence, (S13) is invariant under any transformation of the rates that preserves the microscopic symmetries and the detailed balance condition. Therefore, the occurrence of the dynamical phase transition is robust against any such transformation. Note, however, that the dependence of m_0 on t around t_c [see Fig. 3(f) in the main text] depends on the higher-order terms in \mathcal{H} and $\tilde{\mathcal{H}}$, and may thus be affected by the transformation.

V. DERIVATION OF DYNAMICAL EQUATION OF STATE

We now derive the dynamical equation of state, Eq. (11) in the main text. We start with the Hamiltonian [Eq. (7) in the main text]

$$\mathcal{H}(q, p) = w_+(q)(e^{2p} - 1) + w_-(q)(e^{-2p} - 1), \quad (\text{S22})$$

with N -scaled rates defined in Eq. (S4). To simplify the calculation, we perform the canonical transformation [7] $q \rightarrow \tilde{q}$, $p \rightarrow \tilde{p} + (1/2)d\mathcal{V}_q^{\text{eq}}(q)/dm$. Dropping the tildes, we obtain

$$\mathcal{H}(q, p) = \tau^{-1} \left[\sqrt{1 - q^2} \cosh(2p) - \cosh(\beta_q J q) + q \sinh(\beta_q J q) \right], \quad (\text{S23})$$

with initial conditions $p(0) = d\mathcal{V}^{\text{eq}}[q(0)]/dm - (1/2)d\mathcal{V}_q^{\text{eq}}[q(0)]/dm$ and $q(t) = m$. Close to the critical point, $m_0 \ll 1$ and $m \ll 1$, so that $q(s), p(s) \ll 1$ along the trajectory. This allows us to expand \mathcal{H} as $\mathcal{H} \sim \mathcal{H}_0 + \mathcal{H}_1$, with quadratic and quartic Hamiltonians

$$\tau \mathcal{H}_0 = 2p^2 - \frac{1}{2}\omega_0^2 q^2, \quad \text{and} \quad \tau \mathcal{H}_1 = \frac{2}{3}p^4 - p^2 q^2 - \frac{1}{24}\omega_1^4 q^4, \quad (\text{S24})$$

respectively, and $\omega_0 = J(\beta_c - \beta_q)$, $\omega_1 = J(\beta_q^4 - 4\beta_c\beta_q^3 + 3\beta_c^4)^{1/4}$. We now solve the Hamilton equations $\dot{q} = \partial_p \mathcal{H}(q, p)$, $\dot{p} = -\partial_q \mathcal{H}(q, p)$ perturbatively. To this end, we write $q(s) = q^{(0)}(s) + q^{(1)}(s) + \dots$ and $p(s) = p^{(0)}(s) + p^{(1)}(s) + \dots$ and solve the equation order by order. To lowest order, we obtain the linear equations

$$\tau \frac{d}{dt} \begin{pmatrix} q^{(0)} \\ p^{(0)} \end{pmatrix} = \begin{pmatrix} 0 & 4 \\ \omega_0^2 & 0 \end{pmatrix} \begin{pmatrix} q^{(0)} \\ p^{(0)} \end{pmatrix}, \quad \text{with} \quad q^{(0)}(0) = m_0, \quad p^{(0)}(0) = -\omega_{\text{in}} m_0, \quad (\text{S25})$$

and $\omega_{\text{in}} = J[\beta - (\beta_c + \beta_q)/2]$ follows from the expansion of the initial condition in small m_0 . The lowest order equations are solved by evaluating the matrix exponential. The solution is

$$q^{(0)}(t) = \left[\cosh\left(\frac{2t\omega_0}{\tau}\right) - \frac{2\omega_{\text{in}} \sinh\left(\frac{2t\omega_0}{\tau}\right)}{\omega_0} \right] m_0, \quad p^{(0)}(t) = \frac{1}{2} \left[\omega_0 \sinh\left(\frac{2t\omega_0}{\tau}\right) - 2\omega_{\text{in}} \cosh\left(\frac{2t\omega_0}{\tau}\right) \right] m_0. \quad (\text{S26})$$

Expanding $q^{(0)}(t)$ around t_c we then obtain

$$q^{(0)}(t) = \left\{ -a_1 \left(\frac{t - t_c}{\tau} \right) + \mathcal{O} \left[\left(\frac{t - t_c}{\tau} \right)^2 \right] \right\} m_0, \quad (\text{S27})$$

with

$$a_1 = 2\sqrt{(2\omega_{\text{in}} + \omega_0)(2\omega_{\text{in}} - \omega_0)} = 4J\sqrt{(\beta - \beta_c)(\beta - \beta_q)} > 0. \quad (\text{S28})$$

To compute the next order in perturbation theory, we need to solve the inhomogeneous equations

$$\tau \frac{d}{dt} \begin{pmatrix} q^{(1)} \\ p^{(1)} \end{pmatrix} = \begin{pmatrix} 0 & 4 \\ \omega_0^2 & 0 \end{pmatrix} \begin{pmatrix} q^{(1)} \\ p^{(1)} \end{pmatrix} + \begin{pmatrix} \partial_p \mathcal{H}_1[q^{(0)}, p^{(0)}] \\ -\partial_q \mathcal{H}_1[q^{(0)}, p^{(0)}] \end{pmatrix}, \quad \text{with} \quad q^{(1)}(0) = 0, \quad p^{(1)}(0) = \frac{m_0^3}{6}. \quad (\text{S29})$$

The inhomogeneous equations are solved by first treating in the homogeneous problem, identical to Eqs. (S25) up to the boundary conditions, and then computing the inhomogeneous solution by variation of the constants [8]. The resulting expression for $q^{(1)}$

is lengthy and uninformative. Fortunately, for the approximate dynamical equation of state in the vicinity of the critical point, the lowest order in $t - t_c$ suffices. We find

$$q^{(1)} = \left[b_0 + \mathcal{O}\left(\frac{t-t_c}{\tau}\right) \right] m_0^3, \quad (\text{S30})$$

with

$$b_0 = (48\omega_0^5 a_1)^{-1} \left[32\omega_0^5 - 16\omega_0\omega_{\text{in}}^3 (5\omega_0^4 - 6\omega_0^2 + 12\omega_0\omega_1^4) - 3(\omega_0^4 + 2\omega_0^2 - \omega_1^4)(\omega_0^2 - 4\omega_{\text{in}}^2)^2 t_c \tau^{-1} + 4\omega_0^3\omega_{\text{in}}(3\omega_0^4 + 6\omega_0^2 + 5\omega_1^4) \right]. \quad (\text{S31})$$

Both a_1 and b_0 are positive for $\beta < 3/(2J)$. We note, however, that for $\beta > 3/(2J)$, b_0 is negative for some values of $\beta_q < \beta_c$, and becomes entirely negative for $\beta \gtrsim 1.884$. When b_0 is negative, the next higher order $\propto c_0 m_0^5$ in the equation of state needs to be taken into account. It turns out that $c_0 > 0$ for $\beta < 5/(2J)$, but similarly to b_0 , c_0 becomes negative for $\beta > 5/(2J)$, so that terms of order m_0^7 must be considered. The regions in (β_q, β) -space where different powers of m_0 must be taken into account are shown in Fig. 1(b). At the boundary between the $\propto m_0^3$ and $\propto m_0^5$ regions (solid line) the dynamical phase transition changes from continuous to first order.

In summary, for $\beta < 3/(2J)$ we find the dynamical equation of state, Eq. (11) in the main text,

$$m \sim -[a_1 \tau^{-1}(t - t_c) + \dots] m_0 + (b_0 + \dots) m_0^3, \quad (\text{S32})$$

with $a_1 > 0$ given in Eq. (S27) and b_0 given in Eq. (S31).

-
- [1] R. Courant and D. Hilbert, *Methods of mathematical physics, Volume II* (John Wiley & Sons, 1962).
 - [2] W. H. Press, W. T. Vetterling, S. A. Teukolsky, and B. P. Flannery, *Numerical recipes*, Vol. 818 (Cambridge University Press, Cambridge, 1986).
 - [3] V. A. Kulkarny and B. S. White, *Phys. Fluids* **25**, 1770 (1982).
 - [4] M. Wilkinson and B. Mehlig, *Europhys. Lett.* **71**, 186 (2005).
 - [5] J. Meibohm, K. Gustavsson, J. Bec, and B. Mehlig, *New J. Phys.* **22**, 13033 (2020).
 - [6] M. V. Berry and C. Upstill, *Prog. Opt.* **18**, 257 (1980).
 - [7] H. Goldstein, *Classical Mechanics*, 2nd ed. (Addison-Wesley, Reading, USA, 1980).
 - [8] C. M. Bender and S. A. Orszag, *Advanced Mathematical Methods for Scientists and Engineers* (McGraw-Hill, New York, USA, 1978).